# Feasibility and Advantages of Diffusion Weighted Imaging Atlas Construction in Q-Space

Thijs Dhollander[1,2], Jelle Veraart[3], Wim Van Hecke[1,4,5], Frederik Maes[1,2], Stefan Sunaert[1,4], Jan Sijbers[3], and Paul Suetens[1,2]

[1] Medical Imaging Research Center (MIRC), K.U. Leuven, Leuven, Belgium
[2] Center for Processing Speech and Images (PSI), Department of Electrical Engineering (ESAT), Faculty of Engineering, K.U. Leuven, Leuven, Belgium
[3] Vision Lab, Department of Physics, University of Antwerp, Antwerp, Belgium
[4] Department of Radiology, University Hospitals of the K.U. Leuven, Leuven, Belgium
[5] Department of Radiology, University Hospital Antwerp, Antwerp, Belgium

**Abstract.** In the field of diffusion weighted imaging (DWI), it is common to fit one of many available models to the acquired data. A hybrid diffusion imaging (HYDI) approach even allows to reconstruct different models and measures from a single dataset. Methods for DWI atlas construction (and registration) are as plenty as the number of available models. Therefore, it would be nice if we were able to perform atlas building *before* model reconstruction.

In this work, we present a method for atlas construction of DWI data in q-space: we developed a new multi-subject multi-channel diffeomorphic matching algorithm, which is combined with a recently proposed DWI retransformation method in q-space.

We applied our method to HYDI data of 10 healthy subjects. From the resulting atlas, we also reconstructed some advanced models. We hereby demonstrate the feasibility of q-space atlas building, as well as the quality, advantages and possibilities of such an atlas.

## 1 Introduction

Diffusion weighted imaging (DWI), a magnetic resonance imaging (MRI) technique, is able to provide us with valuable information about tissue microstructure, for instance in the white matter of the brain, by measuring and imaging the self-diffusion of water within this tissue in vivo. Over the years, many models have been proposed to get a grip on the complex information acquired using a DWI protocol. Different models usually have different requirements on the quality and specifications of the acquired data. The recent strategy of hybrid diffusion imaging (HYDI) [1] accounts for this by proposing to acquire data from multiple shells of constant diffusion weighting in q-space. The resulting data (or the appropriate parts of it) can then easily be used for the reconstruction of different models and the calculation of different measures.

Methods for image registration and atlas building are plenty in number, and many have been devised for different (but not all) possible DWI models. The

G. Fichtinger, A. Martel, and T. Peters (Eds.): MICCAI 2011, Part II, LNCS 6892, pp. 166–173, 2011.

unique challenge involved in handling the information in DWI datasets is its orientational dependency. This particular fact renders spatial transformation of these data a difficult challenge of its own: apart from a standard interpolation, an additional reorientation or retransformation step has to be performed in every voxel. This is necessary to keep the information in all voxels in correspondence with the underlying orientational structure of the tissue. Different reorientation and retransformation strategies have already been proposed for some, but again not all, possible models. With the use of all these different models and their own unique registration and atlas building methods, the question also raises to what extent these choices might cause a bias on the results.

All of these problems could potentially be evaded and solved at the same time by being able to perform registration or atlas building *before* the reconstruction of any particular model. The result of such a strategy would have the advantage of still allowing any model to be reconstructed from the same transformed data in q-space. Recently, a method has been proposed to correctly transform raw data (sampled from different shells) in q-space [4]. This effectively opens up the path to registration and atlas building in the raw q-space. In this work, we combine this method with a newly developed multi-subject multi-channel diffeomorphic matching algorithm. The result is a true q-space atlas building method. We then apply this method to HYDI data of 10 healthy subjects. From the resulting atlas, we also reconstruct a selection of some more advanced models.

This work should illustrate the feasibility of q-space atlas construction (or registration) and at the same time highlight the advantages of a resulting q-space atlas by presenting some of its possibilities.

## 2 Methods

### 2.1 Acquisition

Data were acquired from 10 healthy subjects. This was done using a Siemens 3T scanner, with a $2.5\,mm$ isotropic voxel size. A HYDI approach was taken. For each subject, in addition to 10 non-DWI (B0) volumes (which were averaged), 3 different shells of q-space were sampled: 25 gradient directions at $b = 700\,s/mm^2$ ($q = 24.98\,mm^{-1}$), 40 gradient directions at $b = 1000\,s/mm^2$ ($q = 29.85\,mm^{-1}$) and 75 gradient directions at $b = 2800\,s/mm^2$ ($q = 49.96\,mm^{-1}$).

### 2.2 Matching

A new multi-subject multi-channel diffeomorphic matching algorithm was developed in order to match all subjects simultaneously in the average subject (atlas) space. The matching process was guided by 7 "channels", which were calculated straight from the raw data. The $1^{st}$ channel is simply the average B0 of each subject. The other channels are based on the apparent diffusion coefficient (ADC). The ADC of each acquired DWI volume is defined as $ADC = -\ln(S)/b$, where $S$ is its signal intensity normalized by the average B0. The $2^{nd}$, $3^{rd}$ and $4^{th}$ channel consist of the average ADC over each of the 3 shells. The $5^{th}$, $6^{th}$ and

$7^{th}$ channel contain a generalized fractional anisotropy (GFA) measure for each shell, which is calculated as $GFA = \text{std}(ADC)/\,\text{rms}(ADC)$.

The algorithm itself is a combination of diffeomorphic demons [2] and the idea of SyN [3] (no target image, both images deform), extended towards any number of subjects ($N$) and channels ($M$). At each iteration, given the currently deformed subjects $I$, an unconstrained correspondence update field $\vec{U}$ is calculated for every subject $I_i$:

$$\vec{U}(I_i) = \sum_{\substack{1 \leq k \leq M \\ 1 \leq j \leq N \\ j \neq i}} \frac{\vec{V}(I_{i,k}, I_{j,k})}{(N-1)M} \tag{1}$$

This is an average, over all $N-1$ other subjects and $M$ channels, of a force $\vec{V}$ acting between this subject's channel $I_{i,k}$ and the corresponding channel $I_{j,k}$ of another subject. In our case, this results in $9 \times 7 = 63$ force fields acting on each subject at each iteration! The force $\vec{V}$ between 2 images $I$ and $J$ is defined as:

$$\vec{V}(I,J) = -\frac{(I-J)\left(\vec{\nabla}I + \vec{\nabla}J\right)/2}{\left\|\left(\vec{\nabla}I + \vec{\nabla}J\right)/2\right\|^2 + (I-J)^2/(2\epsilon)^2} \tag{2}$$

This symmetric ($\vec{V}(I,J) = -\vec{V}(J,I)$) force incorporates the gradients of both images and has theoretical as well as practical advantages [2]. The parameter $\epsilon$ can be set as the maximum step size.

The algorithm proceeds as diffeomorphic demons, but with every subject treated as a moving entity. In short: a fluid regularization (Gaussian filter) is applied to each $\vec{U}(I_i)$; the diffeomorphic update step (composition of the deformation fields with the fast vector field exponentials of the correspondence update fields) is performed; an elastic/diffusion regularization (Gaussian filter) is applied to each resulting new deformation field. All subject's channels are finally deformed according to the new total deformation fields. The whole process iterates, starting again from calculating (1).

The only parameters are $\epsilon$ and the standard deviations of the regularization kernels. We have them initially all set at 2 (voxels). When convergence is reached, they are all switched to 1, and finally to 0.5.

### 2.3 Deformation and Averaging

Using the final 10 deformation fields obtained from the matching algorithm, the raw acquired volumes are resampled. However, for DWI data, a retransformation step is also needed in each sampled voxel. In [4], it is shown that just reorienting the gradient directions using the forward affine matrix in each voxel produces wrong results, and a correct new method that also preserves isotropic and anisotropic volume fractions is proposed. We apply this method for each of the 3 shells, based on the Jacobian of the deformation fields in each voxel,

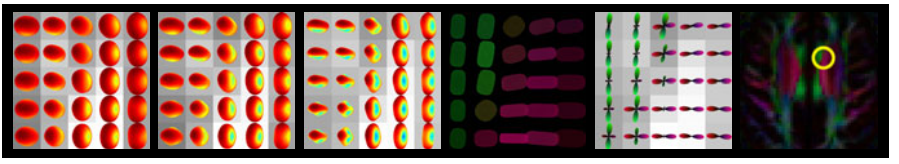

**Fig. 1.** 5x5 voxel detail of the actual atlas (3 analytic shells representing normalized signals in q-space: b700, b1000, b2800). Reconstructed tensors from b1000 as well as fODF's from b2800 are also shown. The region is indicated on an axial slice.

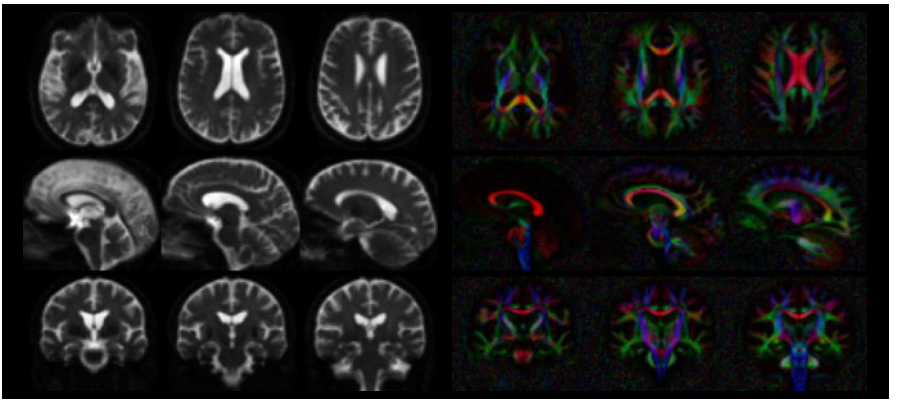

**Fig. 2.** Non-DWI (B0) (*left*) and CFA (*right*) of some axial, sagittal and coronal slices

using an order 6 spherical harmonics (SH) representation of the normalized signal, 1 isotropic and 300 anisotropic volume fractions, shaped by eigenvalues $0.0018\,mm^2/s$ and $0.0003\,mm^2/s$. The resulting SH coefficients of the 3 shells are averaged over all subjects, producing the final atlas: every voxel contains $3 \times 28$ SH coefficients, analytically representing 3 normalized signal shells in q-space. We will further refer to these as b700, b1000 and b2800.

### 2.4 Reconstructions

Apart from a simple tensor fit from diffusion tensor imaging (DTI) and a fiber orientation distribution function (fODF) reconstruction using spherical deconvolution (SD) [5], we will also demonstrate some more advanced reconstructions on the atlas to explore its possibilities to a larger extent. First we will perform a full brain fiber tractography on the fODF's resulting from constrained spherical deconvolution (CSD) [6]. This puts the angular quality of b2800 to the test. Next, we present different parameter maps resulting from a diffusion kurtosis imaging (DKI) model fit on the full atlas [7,8]. This is more of a test for the quality of the radial information, i.e. the relation between the different shells. Finally, we reconstruct the ensemble average propagator (EAP) using the recently proposed multiple q-shell diffusion propagator imaging (mq-DPI) strategy [9]. This technique exploits the full angular and radial information of the atlas.

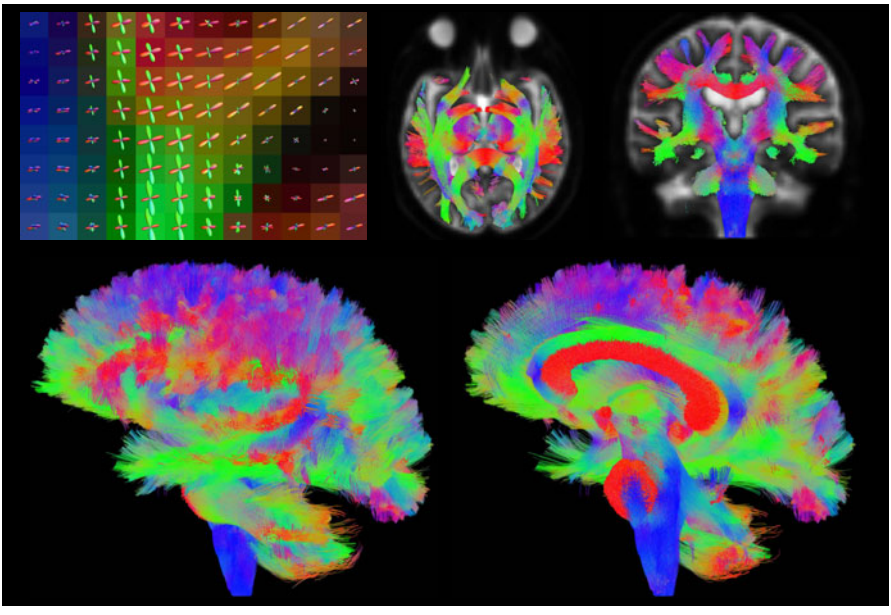

**Fig. 3.** Fiber tracking: fODF's from CSD (*top left*); 10 *mm* thick axial slab (*top middle*) and 3 *mm* thick coronal slab (*top right*) through the tract volume; sagittal view of the full tract volume (*bottom left*) and cut in half by the mid-sagittal plane (*bottom right*)

## 3 Results

In this section, we mainly focus on presenting visualisations of the atlas and its reconstructions, allowing for easy assessment and interpretation of the results.

### 3.1 The Atlas

The atlas itself consists of 3 analytic shells of normalized signals in q-space. For all purposes, these can be sampled along any set of gradient directions, but the SH representations themselves can also prove to be useful (in addition to being a compact representation of the atlas). A small detail (an area where the cingulum and the corpus callosum pass close to each other) of the actual atlas contents is shown in Fig. 1. Already easily exploiting the hybrid nature of the atlas, we also show reconstructed tensors from b1000 and fODF's from b2800 (using SD [5]), as well as some color-encoded fraction anisotropy (CFA) maps in Fig. 2. For the atlas to be complete, we should add the non-DWI volume to it (Fig. 2). If required, it can for instance be used to "de-normalize" samples from the shells, resulting in DWI images as they would be produced by a scanner.

### 3.2 Full Brain Fiber Tractography on fODF's Resulting from CSD

The MRtrix package (http://www.brain.org.au/software/) was used to perform CSD [6] and fiber tracking. To this end, we sampled b2800 in the original 75

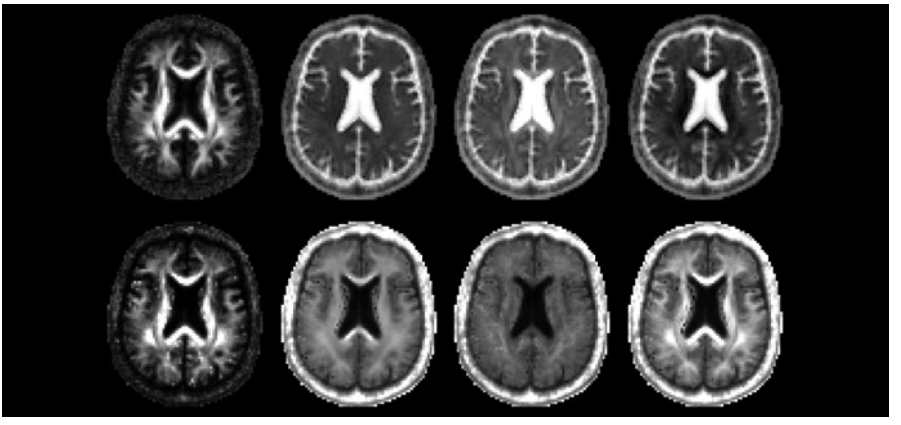

**Fig. 4.** DKI maps: FA, MD, AD, RD (*top row*) and KA, MK, AK, RK (*bottom row*)

directions, and provided this (just as if it were a normal dataset) to MRtrix. We performed CSD using an order 8 SH basis. Even though the atlas itself has only information "up to order 6", this is still useful because CSD is a nonlinear operation: the higher order can be used to fulfill the non-negativity constraint while preserving the quality of the resulting fODF. Fiber tracking was seeded in a white matter mask and constrained to a full brain mask. The fODF amplitude cutoff was 0.25 to initiate tracks and 0.15 to terminate tracks. A stepsize of $0.2\,mm$ and minimum radius of curvature of $1\,mm$ were used. Minimum and maximum track length were set to $15\,mm$ and $300\,mm$. Using these settings, 50000 deterministic and 50000 probabilistic tracks were generated, resulting in a dense 100000 tract volume. Results are shown in Fig. 3.

### 3.3 Parametermaps from DKI

The full atlas was sampled for the original 140 directions and the DKI [7] model was fit to the resulting dataset. DKI accounts for non-Gaussian diffusion (whereas DTI assumes Gaussian diffusion). This allows for an improved and b-value-independent estimation of the classical tensor parameters and at the same time produces some new parameters that quantify the non-Gaussianity [8]. We calculated the classical fractional anisotropy (FA), mean diffusivity (MD), axial diffusivity (AD) and radial diffusivity (RD), as well as the kurtosis anisotropy (KA), mean kurtosis (MK), axial kurtosis (AK) and radial kurtosis (RK). Results are shown in Fig. 4.

### 3.4 Full 3D Signal Fit and the EAP from mq-DPI

Recently, mq-DPI [9] has been proposed as a means of reconstructing the 3D EAP. The idea is to model data of several shells in q-space with solid harmonics (solutions of the Laplace equation in spherical polar coordinates). Using this representation, an analytical solution exists for the Fourier integral that relates the measured signals to the EAP. This time we will use the SH representation

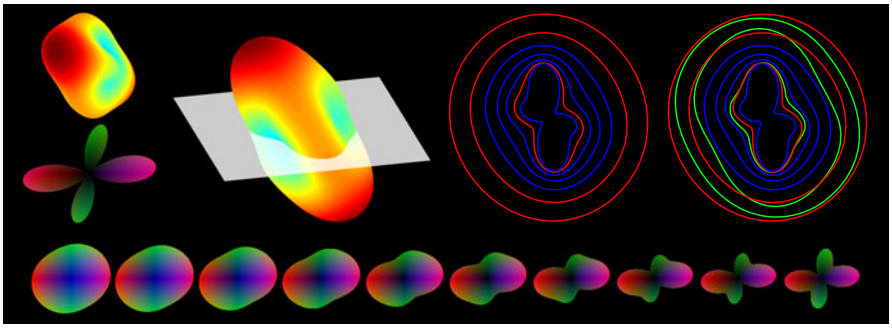

**Fig. 5.** mq-DPI in a single voxel: b2800 shell, fODF, axial plane through the shell (*top left*); solid harmonic fit in the axial plane for $q = 25, 30, 35, 40, 45, 50, 55\, mm^{-1}$ (*from outside to inside*) and with addition of the original b700, b1000, b2800 (*green*) (*top right*); EAP at radii ranging from $12\,\mu m$ to $21\,\mu m$ (*bottom row, left to right*)

of the 3 shells to fit the new model (solid harmonics) to. The implementation described in [9] can easily be adapted for this purpose, as it also implicitly performs a SH fit (but combined with the radial solid harmonic matrices). The final fit describes the signal in function of angle and radius (expressed by the q-value instead of b-value). We used an order 6 fit, modelling our previous $3 \times 28$ with $2 \times 28$ new coefficients. In Fig. 5, we try to give an impression of what such a fit looks like. We picked out a voxel containing a very general setting: 2 fiber populations with a different volume fraction and crossing at a certain angle. A view on the fit inside an axial plane is presented. Using the analytical solution of [9], we also reconstructed the EAP at different radii.

## 4 Discussion and Conclusion

In this work, we presented a method for atlas building of DWI data in the raw q-space. To this end, we combined a newly developed multi-subject multi-channel diffeomorphic matching algorithm with a recently proposed retransformation method [4]. We pursued methods that stay as close as possible to the original data: the channels used in the matching process were all calculated straight from the raw data and the retransformation also operates on the shells in q-space. We should note that the resulting method can just as well be used as a groupwise registration algorithm in different group studies. For the case of 2 subjects, it simply reduces to a (bias/template-free) registration algorithm.

We applied our method to HYDI data of 10 healthy subjects. The result is a DWI atlas, containing analytic representations of 3 shells of q-space data in each voxel. These shells can be sampled for any set of gradient directions, but the analytic SH representations themselves can also be used. We inspected the atlas for its quality and possibilities by performing a simple DTI fit and fODF (from SD [5]) reconstruction, as well as a full brain fiber tractography using fODF's from CSD [6], parametermaps from a DKI model fit [7,8] and a 3D

signal fit and EAP reconstruction from mq-DPI [9]. The outcomes of all these reconstructions are realistic and of good quality. This indicates that the full atlas building method must have brought all subjects in good correspondence, as well spatially as in orientational and radial structure in each voxel. Especially the latter parts are not evident. Because the retransformation is performed as a separate step after the matching and it is very sensitive to the deformation field, a sufficiently smooth deformation field is an absolute requirement. On the other hand, a good matching is of course also necessary. A good balance between both is the key to success. We believe that the fluid and elastic/diffusion regularization *both* play an invaluable part in achieving this.

To conclude, we have shown that DWI atlas construction in q-space is feasible, has advantages and can produce a qualitatively good result.

## References

1. Wu, Y.C., Alexander, A.L.: Hybrid Diffusion Imaging. NeuroImage 36(3), 617–629 (2007)
2. Vercauteren, T., Pennec, X., Perchant, A., Ayache, N.: Diffeomorphic Demons: Efficient Non-parametric Image Registration. NeuroImage 45(1), S61–S72 (2009)
3. Avants, B.B., Epstein, C.L., Grossman, M., Gee, J.C.: Symmetric Diffeomorphic Image Registration with Cross-Correlation: Evaluating Automated Labeling of Elderly and Neurodegenerative Brain. Medical Image Analysis 12(1), 26–41 (2008)
4. Dhollander, T., Van Hecke, W., Maes, F., Sunaert, S., Suetens, P.: Spatial Transformations of High Angular Resolution Diffusion Imaging Data in Q-space. In: MICCAI 13, CDMRI Workshop, pp. 73–83 (2010)
5. Tournier, J.D., Calamante, F., Gadian, D.G., Connelly, A.: Direct Estimation of the Fiber Orientation Density Function from Diffusion-Weighted MRI Data using Spherical Deconvolution. NeuroImage 23(3), 1176–1185 (2004)
6. Tournier, J.D., Calamante, F., Connelly, A.: Robust Determination of the Fibre Orientation Distribution in Diffusion MRI: Non-negativity Constrained Super-resolved Spherical Deconvolution. NeuroImage 35(4), 1459–1472 (2007)
7. Jensen, J.H., Helpern, J.A., Ramani, A., Lu, H., Kaczynski, K.: Diffusional Kurtosis Imaging: The Quantification of Non-Gaussian Water Diffusion by Means of Magnetic Resonance Imaging. MRM 53(6), 1432–1440 (2005)
8. Veraart, J., Poot, D.H.J., Van Hecke, W., Blockx, I., Van der Linden, A., Verhoye, M., Sijbers, J.: More Accurate Estimation of Diffusion Tensor Parameters Using Diffusion Kurtosis Imaging. MRM 65(1), 138–145 (2011)
9. Descoteaux, M., Deriche, R., Le Bihan, D., Mangin, J.F., Poupon, C.: Multiple Q-shell Diffusion Propagator Imaging. Medical Image Analysis (2010) (in press)